Nanomechanics of single and multiwalled carbon nanotubes

K. M. Liew,[1,2,*] C. H. Wong,[1,2] X. Q. He,[1] M. J. Tan,[2] and S. A. Meguid[3]

[1]*Nanyang Centre for Supercomputing and Visualisation, Nanyang Technological University, Nanyang Avenue, Singapore 639798*

[2]*School of Mechanical and Production Engineering, Nanyang Technological University, Nanyang Avenue, Singapore 639798*

[3]*Engineering Mechanics and Design Laboratory, Department of Mechanical and Industrial Engineering, University of Toronto,*
5 King's College Road, Toronto, Ontario, Canada M5S 3G8

Buckling behavior of single-walled and multiwalled carbon nanotubes is studied under axial compression in this work. Brenner's ''second generation'' empirical potential is used to describe the many-body short-range interatomic interactions for single-walled carbon nanotubes, while the Lennard Jones model for the van der Waals potential is added for multiwalled carbon nanotubes. Single-, two-, three-, and four-walled nanotubes are considered in the simulations in order to examine the effects of the number of layers on the structural properties of the multiwalled nanotubes. Results indicate that there exists an optimum diameter for single-walled nanotubes at which the buckling load reaches its maximum value. The buckling load increases rapidly with the increase of the diameter up to the optimum diameter. A further increment beyond this diameter results in a slow decline in buckling load until a steady value is reached. The effects of layers on the buckling load of multiwalled nanotubes are also examined.

I. INTRODUCTION

The discovery of carbon nanotubes in the early 1990's by Iijima[1] has sparked a revolution in chemical physics and materials science in recent years. Since then, much research has been done on these new forms of carbon because of its exceptional mechanical properties. Among these efforts, computer simulations using empirical pair potential are effective methods for the analysis of structural and mechanical properties of complex systems, such as carbon nanotubes. For instance, based on the empirical chemical pseudopotential theory proposed by Abell,[2] Tersoff[3,4] introduced an empirical interatomic potential for complex covalently bonded systems. Using the proposed potential, Tersoff presented a relatively accurate description of the structural properties and energetics of carbon. Brenner[5] developed an empirical many-body potential-energy expression for hydrocarbons by including additional terms into Tersoff's covalent-bonding-order formalism that corrects for an inherent overbinding of radicals. Nonlocal effects are also incorporated in his potential via an analytic function that defines conjugation based on the coordination of carbon atoms that neighboring carbon-carbon bonds. This potential is commonly known as the REBO potential. To model the complex chemistry in large many-body systems, Brenner *et al.*[6] further proposed a so-called ''second-generation'' potential energy expression for solid carbon and hydrocarbon molecules by modifying the analytical functions for the intramolecular interactions and an extended database relative to the earlier version.[5] Their new expression is found to have a significant improvement on (1) yielding of reasonable bond energies, bond lengths and force constants between atoms, (2) allowing for covalent bond breaking and forming, and (3) elastic and plastic behaviors.

The abovementioned developments of many-body interatomic potentials have made molecular dynamics simulations of large systems possible and efficient. Yakobson *et al.*[7]

applied REBO potential to investigate the instability of single-walled carbon nanotubes under the axial compression, bending, and torsional deformation, respectively. In their study, a continuum shell model is also introduced to describe the buckling and bending behavior of nanotubes in the plastic deformation regime by properly chosen parameters. Cornwell and Wille[8,9] carried out a large-scale calculation on the single-walled nanotubes subjected to axial compression and stretched in plastic deformation regime. Instead of using the conjugate-gradient method used by Yakobson *et al.*,[7] Cornwell and Wille used finite temperature molecular dynamic simulation to examine the relaxation of nanotubes. The REBO potential is also employed in their work to describe the interatomic interactions. Using the molecular dynamics simulations as well as the Tersoff many-body potential energy, Erkoc[10] investigated the structural stability of single-walled carbon nanotubes with infinite length and the thermal behavior of three different single-walled carbon nanotubes of similar size, both in diameter and length.[11] The effect of temperature on the structure of nanotubes is examined in their study. In addition, Erkoc *et al.*[12] investigated the stability of finite carbon nanorods formed from multiwalled nanotubes with different chirality. Their simulation results showed that the carbon nanorod is not stable even at low temperatures. The molecular dynamics simulation on the mechanisms of buckling, bending, slipping, and elastic recovery of carbon nanotubes have been carried out by Garg *et al.*[13] Their work investigated the effects of length and surface type of nanotubes on the mechanisms of the interaction between the carbon nanotubes and the surfaces. Also, Garg and Sinnott[14] studied carbon nanotube tip-surface interaction using a many-body empirical hydrocarbon potential coupled to a long-range Lennard-Jones potential. Their simulation indicated how the deformation of the rope leads to the distortion of its end, and allows for the determination of the effect of shear stresses within the bundle on the buckling force of the rope. Hertel *et al.*[15] investigated the effects of surface

van der Waals forces on the shape of single-walled and multiwalled carbon nanotubes using molecular mechanics simulation. Their simulation showed that the van der Waals interaction between nanotubes and a substrate leads to substantial axial and radial deformations of absorbed nanotubes destroying the idealized shape of free tubes. In addition, Ru[16–19] proposed elastic shell models for the buckling analyses of double-walled carbon nanotubes. The derived explicit expression for critical axial strain indicated the role of the van der Waals interaction between the outer and inner tubes. His formula showed that the van der Waals forces do not increase the critical axial strain for infinitesimal buckling of the double-walled carbon nanotube.

The above studies examined the structural deformation associated with mechanical and thermal loads. This paper is complementary to the earlier works by providing a comprehensive study on the buckling behavior of perfectly structured single-walled and multiwalled carbon nanotubes under compressive deformation. The solution to this problem is made possible by employing the molecular dynamic simulation technique, using Brenner's "second generation" potential function, which has the advantages of faster computational time and the ability to simulate large systems with more than 200 atoms, while maintaining the accuracies of semiempirical and *ab initio* methods. In this study, we also computed the optimum diameter of a single-walled carbon nanotube at its maximum buckling load, and investigated the effect of the number of layers in a multiwalled carbon nanotube on its properties during buckling. The spontaneous plastic collapse of the nanotubes from the simulation is in qualitative agreement with the experimental observations of Lourie *et al.*[20] and the simulated observations of Srivastava *et al.*[21] using the quantum generalized tight binding method.

II. NUMERICAL SIMULATIONS AND DISCUSSION

The entire numerical simulations are carried out using the classical molecular dynamics method[22] in which Newtonian equations of motion are solved numerically for a set of atoms interacting via Brenner's "second generation" reactive empirical many-body bond order potential energy.[6] In this study, the buckling behavior of single-walled and multiwalled carbon nanotubes are simulated by solving the equations of motions using the Gear's predictor-corrector algorithm.[23] The axial compression of perfectly structured single-walled and multiwalled carbon nanotubes is achieved by applying a rate of 20 and 10 m/s, respectively, at both ends. At the same time, the atoms at both ends of the nanotube are kept transparent to the interatomic forces. The end atoms are then moved inwardly along the axis by small steps, followed by a conjugate gradient minimization method whilst keeping the end atoms fixed.

A. Single-walled carbon nanotubes

To characterize the buckling behavior of single-walled carbon nanotubes, a (8,0) single-walled carbon nanotube is used in the simulation. The nanotube has a length $l = 43$ Å
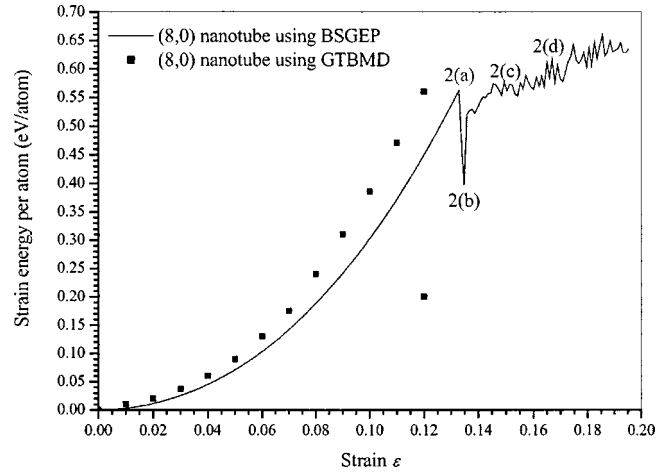
FIG. 1. Computed strain energy per atom for (8,0) single-walled carbon nanotubes using Brenner's "second generation" empirical potential (BSGFP) (Ref. 6) and (8,0) single-walled carbon nanotube using GTBMD (Ref. 21).

and diameter $d = 6.3$ Å. Each time step used in this simulation is equivalent to 1 fs and the simulations are allowed to run for 20 000 time steps.

Figure 1 shows the plot of strain energy per atom, which is determined as the difference in total energy per atom of the strained and unstrained carbon nanotube, against strain, which is defined as the ratio of elongation/original length for the (8,0) carbon nanotubes after it is compressed axially using the Brenner's second generation empirical potential function.[6] In addition, for comparison, the similar strain energy calculated for (8,0) carbon nanotube using quantum generalized tight-binding molecular dynamics (GTBMD)[21] is also shown. At the elastic regime, both Brenner's second generation empirical analytical potential function and the GTBMD simulation agrees well (only with a slight difference). Furthermore, Brenner's second generation empirical analytical potential function shows that the (8,0) carbon nanotube can be compressed up to a strain $\varepsilon = 0.13$ before buckling; while the GTBMD simulation for the same nanotube shows that buckling starts at strain $\varepsilon = 0.12$. Hence, generally both the GTBMD and Brenner's second generation empirical analytical potential agrees well with one each other, validating the accuracy of the latter.

Figure 1 depicts that the (8,0) single-walled carbon nanotube undergoes elastic deformation before collapsing catastrophically at a certain critical strain of $\varepsilon = 0.13$, resulting in a 30% spontaneous drop of strain energy per atom to 0.4 eV/atom. The nature of the spontaneous plastic collapse of single-walled nanotubes reported in this paper is in qualitative agreement with the experimental observation of Lourie *et al.*[20] and the simulated observation of Srivastava *et al.*[21] using the GTBMD scheme. The calculated critical stress $\sigma_{cr} = 149$ GPa for the (8,0) single-walled carbon nanotube in this work is also close to the simulation work of Srivastava *et al.*[21] who obtained $\sigma_{cr} = 153$ GPa. The (8,0) carbon nanotube is subjected to acute morphological changes, hence, higher strains are found in the (8,0) carbon nanotube, particularly around the kinks.

(a)   (b)   (c)   (d)
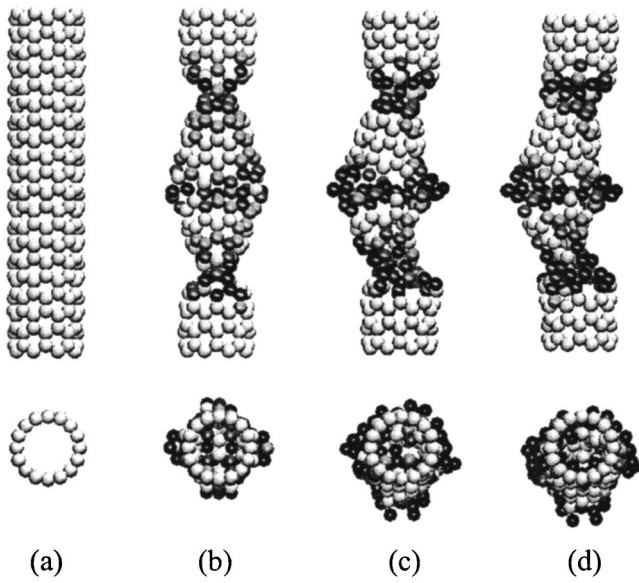
FIG. 2. Morphological changes for (8,0) single-walled nanotube showing high strains concentrated at the kinks. The (8,0) nanotube at $\varepsilon = 0.13$ (a) spontaneously collapse into a three-fin pattern while maintaining its straight axis (b). At $\varepsilon = 0.15$, the nanotube buckles sideways (c) before further reduction in length at $\varepsilon = 0.17$ (d).

In Fig. 2, the shading indicates the strain energy per atom, equally spaced from below 0.25 eV (lightest) to above 1.25 eV (darkest). According to Fig. 2(a), at $\varepsilon = 0.13$ the compressed (8,0) carbon nanotube maintains its cylindrical shape before spontaneously deforming into a symmetric three-fin pattern as shown in Fig. 2(b), leading to a plastic collapse and a net release of energy. This phenomenon has also been discussed by Srivastava *et al.*[21] The highly symmetric morphological shape is intrinsic to the mechanics of a perfect,

undisturbed carbon nanotube as reported.[7,21] Furthermore, higher strain energy per atom is found along the edges of the fin. At $\varepsilon = 0.15$, the nanotube continues to deform with the pinches thinning while buckling sideways, as shown in Fig. 2(c). It is observed that high strain energy per atom is located across the pinch as the nanotube is being compressed. Further increase in strain beyond $\varepsilon = 0.17$ causes the nanotube to continue to buckle sideways with further reduction in length l, as shown in Fig. 2(d), where high strain energy per atom is concentrated at the kinks.

A length/diameter (l/d) ratio of 7.7:1 is used to illustrate its relationship with the buckling loads P_{cr} of selected zig-zag and armchair single-walled carbon nanotubes listed in Table I. From the table, it is observed that as the diameters d increase, the buckling loads P_{cr} also increase steadily until the optimum diameters of $d = 11.76$ Å and $d = 20.36$ Å for the zig-zag and armchair nanotubes, respectively, were attained. Beyond these optimum diameters d, the buckling loads P_{cr} start to decrease instead. It is, however, important to note that for any l/d ratio, there is an optimum diameter.

For clarity, Fig. 3 shows the plot of buckling load P_{cr} against diameter d for zig-zag single-walled carbon nanotubes. As the diameter d of the zig-zag nanotube increases, there is a rapid increase in its buckling load P_{cr}. However, as the diameter d reaches an optimum value $d = 11.76$ Å, any further increment beyond that will cause the buckling load P_{cr} to decrease slowly to a steady value of about 1.10×10^{-7} N. It is evident that the length l of the carbon nanotubes will affect the critical strain ε_{cr}.

It is worthy to note that the classical shell theory can be used for the local buckling analysis of nanotubes. For a layer of cylindrical shell with length l, radius r, thickness t, Young's modulus E, Poisson's ratio ν, and m and $2n$ longitudinal and circumferential wave numbers, the critical stress for the buckling of the cylindrical shell is obtained as[24]

TABLE I. Buckling loads for selected zig-zag and armchair single-walled carbon nanotubes.

	Zig zag						Armchair				
(n,m)	Diameter d (Å)	P_{cr} ($\times 10^{-7}$ N)	(n,m)	Diameter d (Å)	P_{cr} ($\times 10^{-7}$ N)	(n,m)	Diameter d (Å)	P_{cr} ($\times 10^{-7}$ N)	(n,m)	Diameter d (Å)	P_{cr} ($\times 10^{-7}$ N)
(4,0)	3.13	0.72	(20,0)	15.67	1.25	(4,4)	5.43	0.87	(20,20)	27.15	1.19
(5,0)	3.92	0.94	(21,0)	16.46	1.24	(5,5)	6.79	0.88	(21,21)	28.50	1.17
(6,0)	4.70	1.01	(22,0)	17.24	1.23	(6,6)	8.14	0.90	(22,22)	29.86	1.16
(7,0)	5.49	1.09	(23,0)	18.02	1.21	(7,7)	9.50	0.90	(23,23)	31.22	1.16
(8,0)	6.27	1.10	(24,0)	18.81	1.18	(8,8)	10.86	0.91	(24,24)	32.58	1.15
(9,0)	7.05	1.14	(25,0)	19.59	1.16	(9,9)	12.22	1.03	(25,25)	33.93	1.14
(10,0)	7.84	1.19	(26,0)	20.38	1.15	(10,10)	13.57	1.04	(26,26)	35.29	1.12
(11,0)	8.62	1.20	(27,0)	21.16	1.14	(11,11)	14.93	1.12	(27,27)	36.65	1.11
(12,0)	9.40	1.22	(28,0)	21.94	1.14	(12,12)	16.29	1.13	(28,28)	38.01	1.11
(13,0)	10.19	1.25	(29,0)	22.73	1.13	(13,13)	17.65	1.15	(29,29)	39.36	1.10
(14,0)	10.97	1.27	(30,0)	23.51	1.12	(14,14)	19.00	1.16	(30,30)	40.72	1.09
(15,0)	11.76	1.30	(35,0)	27.43	1.11	(15,15)	20.36	1.16	(32,32)	43.44	1.09
(16,0)	12.54	1.29	(40,0)	31.35	1.10	(16,16)	21.72	1.18	(34,34)	46.15	1.09
(17,0)	13.32	1.27	(45,0)	35.27	1.10	(17,17)	23.08	1.19	(35,35)	47.51	1.09
(18,0)	14.11	1.26	(50,0)	39.18	1.09	(18,18)	24.43	1.19	(37,37)	50.22	1.09
(19,0)	14.89	1.25	(55,0)	43.10	1.09	(19,19)	25.79	1.20	(40,40)	54.29	1.09
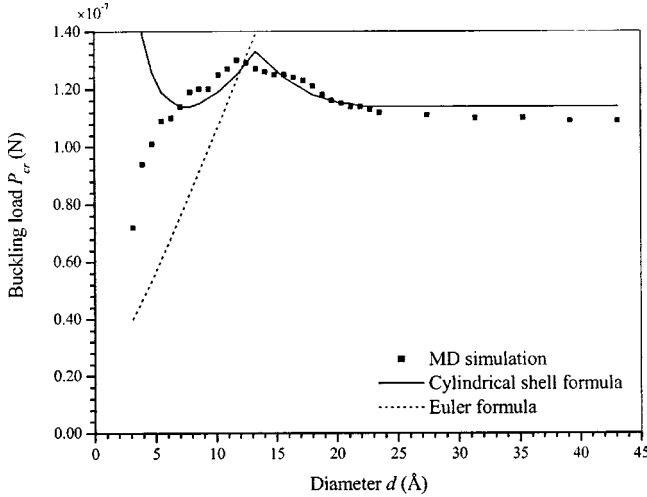
FIG. 3. Comparison between cylindrical shell formula and molecular dynamics simulation for buckling loads P_{cr} of various zig-zig single-walled nanotubes with different diameters

$$\sigma_{cr} = \frac{Et^3}{12(1-\nu^2)} \left\{ \frac{[n^2 + (m^2\pi^2 r^2/l^2)]^2}{r^2(m^2\pi^2 r^2/l^2)} \right\} + \frac{E(m^2\pi^2 r^2/l^2)}{[n^2 + (m^2\pi^2 r^2/l^2)]^2}. \tag{1}$$

In predicting the buckling load of nanotubes by using the cylindrical shell model, almost all previous literatures adopted the interlayer separation of graphite, i.e., $t = 3.4$ Å as the representative thickness of single-walled nanotubes. However, the buckling loads obtained from Eq. (1) are much larger than our molecular dynamics simulated results if $t = 3.4$ Å is used. Here, we took the diameter of carbon atom (1.54 Å) as the thickness of the nanotube, as shown in Fig. 2(a). The Young modulus $E = 1.28$ TPa is directly extracted from the experimental results of Wong *et al.*[25] for the calculation of buckling loads using Eq. (1). The buckling load is not sensitive to the value of Poisson's ratio, thus in this study, it is taken as $\nu = 0.25$. Using the cylindrical shell formula in Eq. (1) and molecular dynamics, buckling loads are computed for various zig-zig single-walled nanotubes, as shown in Fig. 3. It is observed from Fig. 3 that the two sets of results are in good agreement with diameter d ranging from 5.49 to 43.1 Å or larger. In spite of this, the results obtained from the cylindrical shell formula [Eq. (1)] for diameters d smaller than 4.7 Å do not agree well with that of the molecular dynamics simulation. This is because the nanotube behaves more similar to a rod than a cylindrical shell with thickness/radius (t/r) ratio larger than 0.66. In view of this, the buckling loads of zig-zag nanotubes with fixed ends are also calculated using Euler's formula[26] and are presented in Fig. 3,

$$P_{cr} = \frac{4\pi^2 EI}{l^2}, \tag{2}$$

where I is the moment of inertia. For the fixed length/diameter (l/d) ratio, the buckling loads obtained from
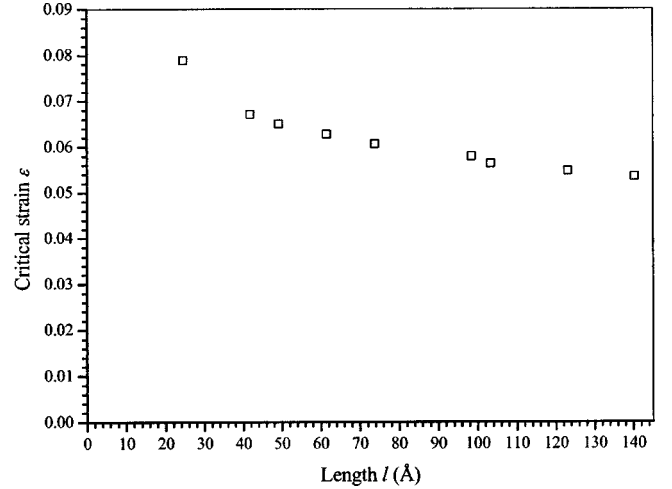
FIG. 4. Critical strains ε_{cr} for (10,10) single-walled carbon nanotubes with diameter of 13.57 Å at different lengths l.

Euler's formula for nanotubes with fixed ends are proportional to the diameter d of nanotubes, as shown in Fig. 3. It is obvious from the trend that the Euler formula is more reasonable than the cylindrical shell model in the estimation of the buckling loads of nanotubes with (t/r) ratio larger than 0.66.

Figure 4 plots the various critical strains ε_{cr} of a (10,10) single-walled carbon nanotube at different lengths l from 24.6 to 140.0 Å. This plot shows that as the length l increases, the critical strain ε_{cr} decreases. This indicates that a larger l/d ratio results in a lower critical strain ε_{cr}.

B. Multiwalled carbon nanotubes

Comparisons are also made between multiwalled carbon nanotubes to determine the effect of the number of layers on the properties of the multiwalled nanotubes. Three configurations of multiwalled nanotubes are considered in the simulation: the first is a two-walled (5,5) and (10,10) nanotube; the second is a three-walled (5,5), (10,10), and (15,15) nanotube; and the last is a four-walled (5,5), (10,10), (15,15), and (20,20) nanotube. The lengths of all three multiwalled nanotubes are $l = 60$ Å. And their diameters d are 13.52, 20.36, and 27.15 Å for the two-, three-, and four-walled nanotubes, respectively. In these simulations, the long-range van der Waals potential is added into the short-range covalent potential for the interlayer interaction using the Lennard-Jones 12-6 potential[27]

$$V_{ij}(r_{ij}) = 4\frac{\xi}{\sigma}\left[\left(\frac{\sigma}{r_{ij}}\right)^{12} - \left(\frac{\sigma}{r_{ij}}\right)^6\right], \tag{3}$$

where the coefficients of well-depth energy ξ and the equilibrium distance σ are 4.2038×10^{-3} eV and 3.4 Å, respectively.[28]

It is worthy to note that the van der Waals potential is nonzero only if the covalent potential is zero, such that there is no artificial reaction barrier formed by the steep repulsive wall of the Lennard-Jones 12-6 potential to prevent nonbonded atoms from chemical reactions. The three multi-
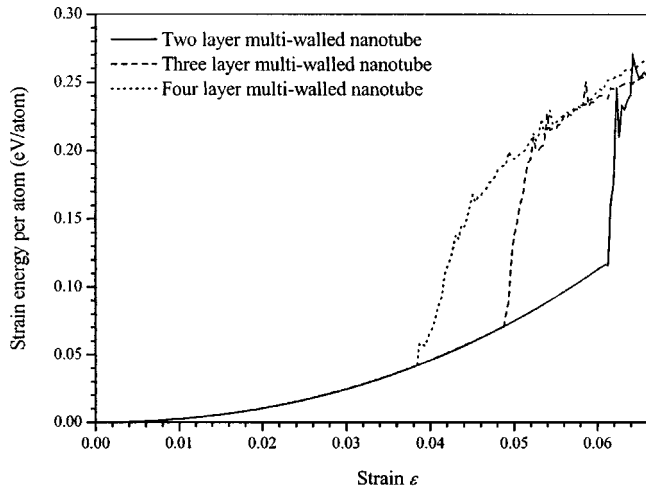
FIG. 5. Strain energy per atom for two layers [(5,5) and (10,10) with diameter of 13.57 Å], three layers [(5,5), (10,10), and (15,15) with diameter of 20.36 Å], and four layers [(5,5), (10,10), (15,15), and (20,20) with diameter of 27.15 Å] multiwalled carbon nanotubes.

walled nanotubes are compressed axially using the same method as the single-walled nanotubes. Each time step is equivalent to 1 fs and there are a total of 20 000 time steps, which corresponds approximately to $\varepsilon = 0.066$. The resulting plots are shown in Fig. 5. For multiwalled nanotubes with m layers, the total strain energy is

$$E_s = \sum_{i}^{m} E_i . \qquad (4)$$

Figure 5 depicts that the two-walled carbon nanotube manages to keep its elasticity for the longest with the largest critical strain at $\varepsilon = 0.06$, whilst the four-walled carbon nanotube has the lowest critical strain at $\varepsilon = 0.038$. Instead of a spontaneous decrease of strain energy upon buckling as evidenced in the single-walled carbon nanotubes, the strain en-
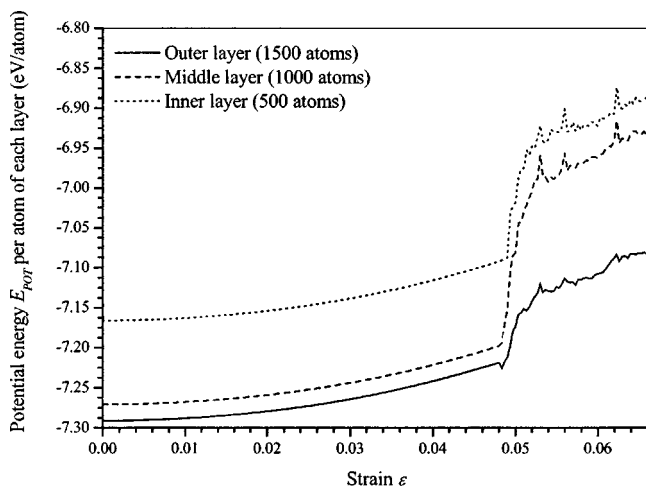
FIG. 6. Potential energy per atom for each layer for (5,5), (10,10), and (15,15) three-walled carbon nanotube with diameter 20.36 Å.
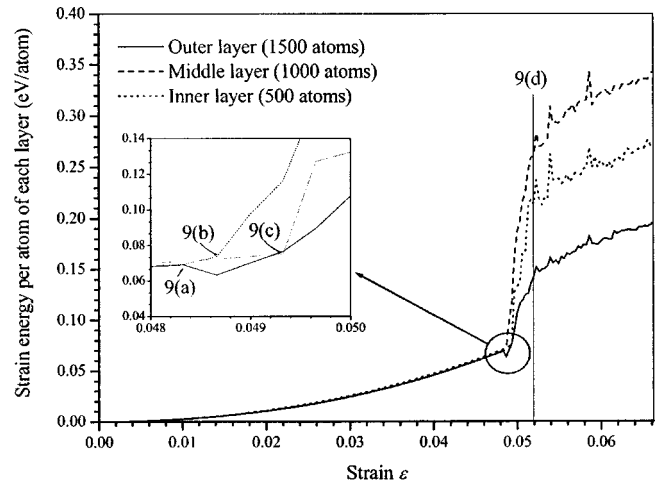
FIG. 7. Strain energy per atom of each layer for (5,5), (10,10), and (15,15) three-walled carbon nanotube with diameter 20.36 Å.

ergy per atom increases until all the layers in the multiwalled carbon nanotubes are fully buckled.

The sudden increase in strain energy per atom for each layer is due to the spontaneous increase in potential energy of each atom for each layer as depicted in Fig. 6. From the plot, it is observed that the middle layer has the largest increment of potential energy of each atom for each layer followed by the inner layer and then the outer layer. Being sandwiched between the outer and inner layer, when the three-walled carbon nanotube starts to buckle, the atoms at the middle layer will have more nearest neighbors than those of the outer and inner layer. This causes the formation of more chemical bonds to form, from sp^2 to sp^3 configurations. Thus, it leads to a larger increase in the empirical bond order function and consequently the potential energy. Hence the middle layer has the highest strain energy per atom for each layer after buckling, as seen in Fig. 7.
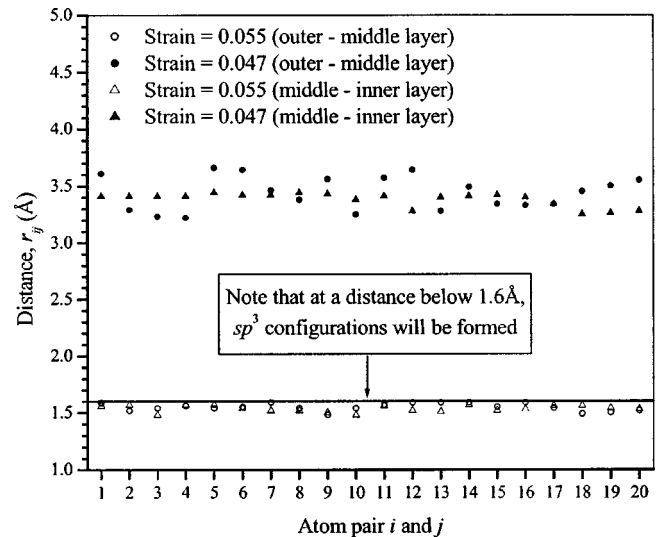
FIG. 8. Distances between atoms from different layers before buckling at $\varepsilon = 0.047$ and after buckling at $\varepsilon = 0.055$ for the three-walled carbon nanotube.
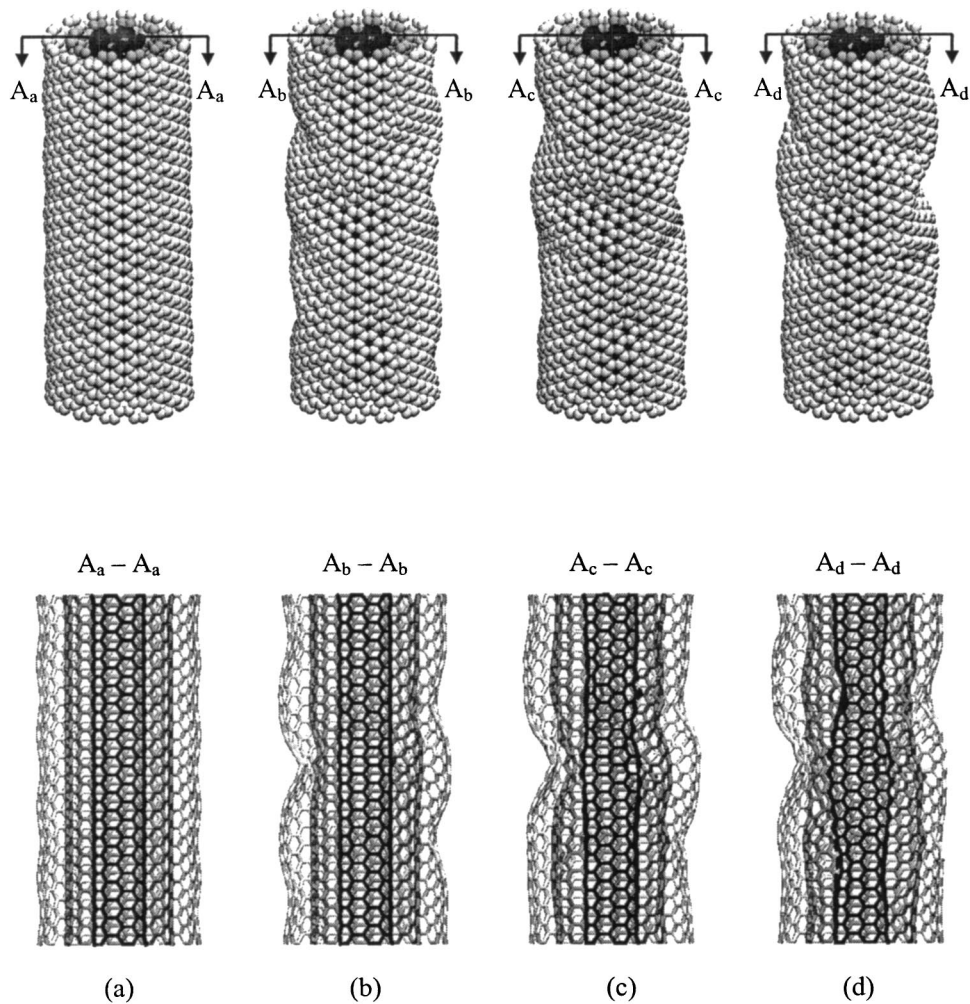
FIG. 9. Three-dimensional and cross-sectional view of morphological changes for three-walled (5,5), (10,10), and (15,15) carbon nanotube with diameter 20.4 Å. At $\varepsilon = 0.0484$ the outer layer deforms into a "ring" pattern (a). Further compression at $\varepsilon = 0.0486$ causes the middle later to deform too (b). At $\varepsilon = 0.0493$, the inner layer also buckles (c) and at $\varepsilon = 0.052$, all the three layers are deformed (d)
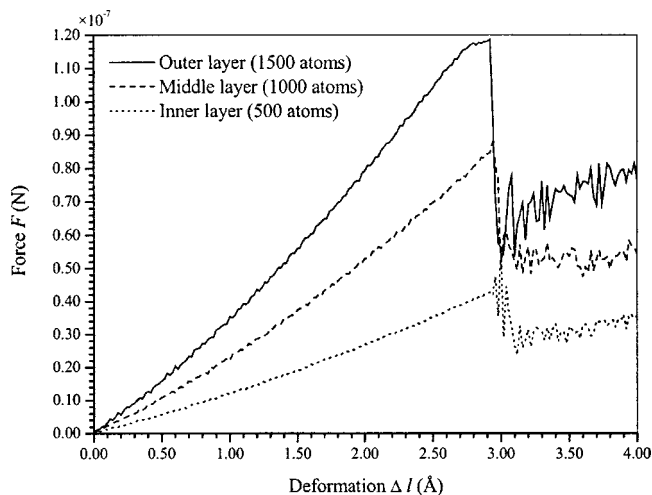
FIG. 10. Force-deformation curves of each layer for (5,5), (10,10), and (15,15) three-walled carbon nanotube with diameter 20.4 Å.
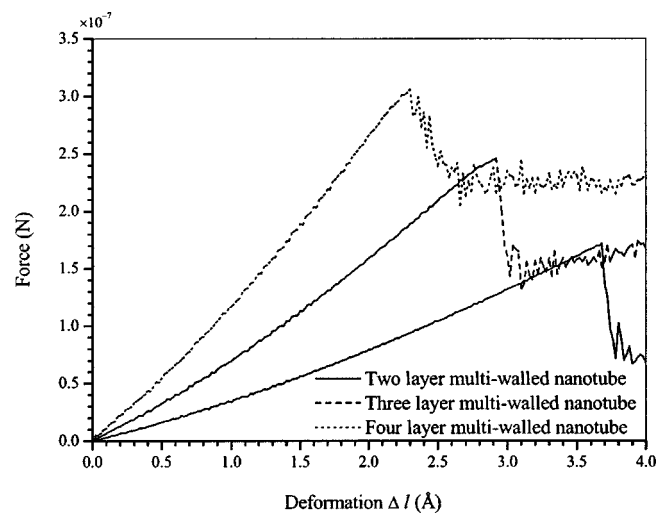
FIG. 11. Force-deformation curves for two layers [(5,5) and (10,10) with diameter of 13.57 Å], three layers [(5,5), (10,10), and (15,15) with diameter of 20.36 Å], and four layers [(5,5), (10,10), (15,15), and (20,20) with diameter of 27.15 Å] multiwalled carbon nanotubes.

TABLE II. Buckling loads for selected two and three-walled carbon nanotubes.

Two-walled		Three-walled	
(n_1,m_1) (n_2,m_2)	P_{cr} $(\times 10^{-7}\ N)$	(n_1,m_1) (n_2,m_2) (n_3,m_3)	P_{cr} $(\times 10^{-7}\ N)$
(5,5) (10,10)	1.72	(5,5) (10,10) (15,15)	2.46
(10,10) (15,15)	2.02	(10,10) (15,15) (20,20)	2.73
(15,15) (20,20)	2.09	(15,15) (20,20) (25,25)	2.81
(20,20) (25,25)	2.10	(20,20) (25,25) (30,30)	3.05

Figure 8 depicts the distances of a selective pair of atoms from different layers at $\varepsilon = 0.047$ (before buckling) and $\varepsilon = 0.055$ (after buckling) of the three-walled carbon nanotube. It is observed that at $\varepsilon = 0.047$, the distances between the atoms from different layers are approximately 3.4 Å apart. However, at $\varepsilon = 0.055$, the distances between these atoms are reduced to values less than 1.6 Å. The decrease in distance allows the formation of sp^3 bond that results in a rise in the potential energy.

To further explain the phenomenon of the increase in strain energy per atom upon buckling as observed in Fig. 5, the plot of the strain energy per atom for each layer of the three-walled nanotube against the strain ε is presented in Fig. 7. Before buckling, the three layers have the same strain energy per atom for each layer. However, at $\varepsilon = 0.0484$ the outer layer starts to buckle first, followed by the middle layer at $\varepsilon = 0.0486$, and then inner layer at $\varepsilon = 0.0493$ (see the inset of Fig. 7 for amplification).

Figure 9 shows the three-dimensional and cross-sectional three-walled nanotube at different strains. It is evident from Fig. 9(a) that the outer layer starts to deform first into a ring pattern at $\varepsilon = 0.0484$, while the middle and inner layers are undeformed and their strain energies remain low. However, further compression at $\varepsilon = 0.0486$ causes the middle layer to deform too, resulting in a sudden increase in the strain energy per atom because of the increase in potential energy due to the atoms in the middle layer. Similarly at this time, the inner layer maintains the elasticity of the nanotube temporarily as shortly after at $\varepsilon = 0.0493$, the inner layer also starts to buckle, therefore increasing the overall potential energy and hence further increasing the strain energy per atom further. After $\varepsilon = 0.052$, all the layers are deformed, hence there is no further abrupt increase in potential energy due to any sudden addition of nearest neighbors.

The force-deformation plot in Fig. 10 shows the buckling load P_{cr} that each layer is able to withstand. Being a layer with a wider diameter d, the outer layer of the three-walled carbon nanotube has the highest bucking load P_{cr} at about 1.18×10^{-7} N. However, it also tends to buckle fractionally earlier than the other two layers after deforming $\Delta l = 2.9$ Å. The buckling loads P_{cr} for the middle and inner layers are lower at 0.88×10^{-7} N and 0.42×10^{-7} N, respectively.

According to Fig. 11, the buckling load P_{cr} increases as the number of layers in a multiwalled nanotube increases. The four-walled nanotube buckles first at $\Delta l = 2.3$ Å even though it has the highest buckling load P_{cr} at 3.2×10^{-7} N;

while the three-walled nanotube buckles at $\Delta l = 2.9$ Å with $P_{cr} = 2.5 \times 10^{-7}$ N. And finally, the two-walled nanotube buckles last at $\Delta l = 3.7$ Å but with the lowest buckling load $P_{cr} = 1.7 \times 10^{-7}$ N. Hence the more layers a multiwalled nanotube has, the higher the buckling load P_{cr} is required.

The buckling loads P_{cr} for two and three-walled carbon nanotubes are tabulated in Table II. It is observed from the table that generally multiwalled carbon nanotubes have larger buckling loads P_{cr}. For instance, the (10,10), (15,15) two-walled carbon nanotube has a higher buckling load $P_{cr} = 2.02 \times 10^{-7}$ N compared to the (5,5), (10,10) two-walled carbon nanotube that has a buckling load $P_{cr} = 1.72 \times 10^{-7}$ N (see Table II). Moreover, Table II also verifies that as the number of layers in a carbon nanotube increases, its buckling load P_{cr} increases too. According to Table I, the buckling load P_{cr} for a (5,5) single-walled carbon nanotube is 0.88×10^{-7} N. However, if an extra outer layer is added to form a (5,5), (10,10) two-walled carbon nanotube, its buckling load P_{cr} increases to 1.72×10^{-7} N as seen in Table II. If another layer is added to form a (5,5), (10,10), and (15,15) three-walled carbon nanotube, the buckling load P_{cr} increases to 2.46×10^{-7} N.

III. CONCLUSIONS

The molecular dynamics simulation technique was used to analyze the structural properties of the single-walled and multiwalled nanotubes. The buckling loads for a number of single-walled and multiwalled carbon nanotubes are determined in the study. The calculations show that as the diameter of single-walled nanotubes increases, the buckling load P_{cr} increases rapidly up to an optimum buckling load P_{cr}. Any further increase beyond the optimum diameter d, however, will result in a slow decline in buckling load P_{cr} up to a steady value. Therefore, each single-walled carbon nanotube has an optimum diameter d that yields the highest buckling load P_{cr}. In addition, the number of layers in a multiwalled nanotube will also affect its structural properties. When a single-walled carbon nanotube buckles, there is a sudden decrease in strain energy, however, when a multiwalled carbon nanotube buckles, there is a spontaneous increase in strain energy. This is due to the growth of potential energy as more chemical bonds change from sp^2 to sp^3 configurations.

*Email address: mkmliew@ntu.edu.sg

[1] S. Iijima, Nature (London) **354**, 56 (1991).

[2] G. C. Abell, Phys. Rev. B **31**, 6184 (1985).

[3] J. Tersoff, Phys. Rev. Lett. **56**, 632 (1986).

[4] J. Tersoff, Phys. Rev. B **37**, 6991 (1988).

[5] D. W. Brenner, Phys. Rev. B **42**, 9458 (1990).

[6] D. W. Brenner, O. A. Shenderova, J. A. Harrison, S. J. Stuart, B. Ni, and S. B. Sinnott, J. Phys.: Condens. Matter **14**, 783 (2002).

[7] B. I. Yakobson, C. J. Brabec, and J. Bernholc, Phys. Rev. Lett. **76**, 2511 (1996).

[8] C. F. Cornwell and L. T. Wille, Solid State Commun. **101**, 555 (1997).

[9] C. F. Cornwell and L. T. Wille, Comput. Mater. Sci. **10**, 42 (1998).

[10] S. Erkoc, Int. J. Mod. Phys. C **11**, 547 (2000).

[11] S. Erkoc, Int. J. Mod. Phys. C **12**, 865 (2001).

[12] S. Erkoc and O. B. Malicioglu, Int. J. Mod. Phys. C **13**, 367 (2002).

[13] A. Garg, J. Han, and S. B. Sinnott, Phys. Rev. Lett. **81**, 2260 (1988).

[14] A. Garg and S. B. Sinnott, Phys. Rev. B **60**, 13 786 (1999).

[15] T. Hertel, R. E. Walkup, and P. Avouris, Phys. Rev. B **58**, 13 870 (1998).

[16] C. Q. Ru, J. Mech. Phys. Solids **49**, 1265 (2001).

[17] C. Q. Ru, Phys. Rev. B **62**, 10 405 (2000).

[18] C. Q. Ru, J. Appl. Phys. **87**, 7227 (2000).

[19] C. Q. Ru, Phys. Rev. B **62**, 9973 (2000).

[20] O. Lourie, D. M. Cox, and H. D. Wagner, Phys. Rev. Lett. **81**, 1638 (1998).

[21] D. Srivastava, M. Menon, and K. Cho, Phys. Rev. Lett. **83**, 2973 (1999).

[22] M. W. Ribarsky and U. Landman, Phys. Rev. B **38**, 9522 (1988).

[23] C. W. Gear, *Numerical Initial Value Problems in Ordinary Differential Equations* (Prentice-Hall, New Jersey, USA, 1971), Chap. 9.

[24] H. G. Allen and P. S. Bulson, *Background to Buckling* (McGraw-Hill, London, 1980), Chap 7.

[25] E. W. Wong, P. E. Sheehan, and C. M. Lieber, Science **277**, 1971 (1997).

[26] S. P. Timoshenko and James M. Gere, *Mechanics of Materials* (Van Nostrand Reinhold Company, New York, 1973), Chap. 10.

[27] L. E. Lennard-Jones, Proc. R. Soc. London, Ser. A **106**, 441 (1924); **106**, 463 (1924).

[28] M. A. Moller, D. J. Tildesley, K. S. Kim, and N. Quirke, J. Chem. Phys. **94**, 8390 (1991).